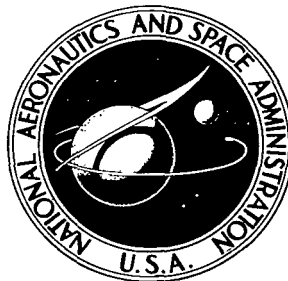


NASA TECHNICAL NOTE



NASA TN D-5062

*c. 1*

NASA TN D-5062



LOAN COPY: RETURN TO  
AFWL (WLIL-2)  
KIRTLAND AFB, N MEX

REQUIREMENTS OF A MARTIAN  
TELEVISION EXPERIMENT FOR THREE  
POINT-MASS DESCENT TRAJECTORIES

*by Friedrich O. Huck, Leonard P. Kopia,  
and Robert B. Spiers, Jr.*

*Langley Research Center  
Langley Station, Hampton, Va.*



REQUIREMENTS OF A MARTIAN TELEVISION EXPERIMENT

FOR THREE POINT-MASS DESCENT TRAJECTORIES

By Friedrich O. Huck, Leonard P. Kopia,  
and Robert B. Spiers, Jr.

Langley Research Center  
Langley Station, Hampton, Va.

NATIONAL AERONAUTICS AND SPACE ADMINISTRATION

---

For sale by the Clearinghouse for Federal Scientific and Technical Information  
Springfield, Virginia 22151 - CFSTI price \$3.00

# REQUIREMENTS OF A MARTIAN TELEVISION EXPERIMENT FOR THREE POINT-MASS DESCENT TRAJECTORIES

By Friedrich O. Huck, Leonard P. Kopia,  
and Robert B. Spiers, Jr.  
Langley Research Center

## SUMMARY

An analytical approach is used to specify the transmission rate and field-of-view requirements of a television experiment on board a spacecraft as it descends through the Martian atmosphere to land a surface laboratory. The objectives of this experiment are to provide a chain of overlapping images between orbiter and surface-laboratory pictures and a 1-meter-resolution survey of the landing site before impact.

Preliminary estimates of the requirements and prediction of the performance are based on three point-mass trajectories, which are the result of numerical integrations of the spacecraft motion through two different Martian atmospheric models. It is found that a single television system can achieve the experiment objectives. For a 200-line television system, the required transmission rates range from  $1.4 \times 10^5$  to  $2.7 \times 10^5$  bits per second, and the fields of view range from  $12^\circ$  to  $22^\circ$ , depending on the descent trajectory and the camera viewing direction. This required transmission rate may be halved by employing two television systems.

## INTRODUCTION

Imagery experiments by unmanned spacecraft provide a valuable tool for the scientific exploration of the planets. Such experiments are particularly suited to Mars exploration, where the thin and sparsely clouded atmosphere allows both mapping by an orbiter and high-resolution surveillance by a surface laboratory. As shown by the Lunar Orbiter and Surveyor programs, the information derived from visual mapping by an orbiter and high-resolution surveillance by a surface laboratory is greatly enhanced if it can be correlated by the precise location of the landing site in the pictures obtained from the orbiter. However, in the case of Mars, neither the surface-laboratory structure nor the area covered by the landed imaging system is likely to be detectable in the pictures obtained from an orbiter, since orbit periapsis cannot be designed significantly lower than 500 kilometers and still comply with the planetary sterilization requirement for an orbit lifetime of at least 50 years. Even Lunar Orbiter's telephoto lens and high-definition

film system barely detected the Surveyor spacecraft on the lunar surface from an altitude of only 50 kilometers (ref. 1). Also, the descent trajectory data may not permit accurate location of the landing site.

One approach for precisely locating the landing point would be to establish an image link between the pictures from the orbiter and the surface laboratory with a television system on board the entry vehicle as it descends through the Martian atmosphere. Such a link would consist of a chain of overlapping images, of which the initial image can be detected in the orbiter pictures and the final image can be correlated to the surface-laboratory pictures. This image chain would also provide Martian surface information on a scale (area coverage and resolution) between that received from the orbiter and the surface laboratory. In addition, since the possibility of a landing failure cannot be disregarded, this television system could secure an image of the landing site shortly before touchdown with a resolution sufficient to reveal any surface obstacles which could cause such a failure. In this event, these images would provide a closer view of the Martian surface than could be obtained from the orbiter pictures.

In the design of a television system for the impacting mission of the Ranger spacecraft to obtain high-resolution pictures of the lunar surface, lunar luminance and approach velocity and the resulting image smear were paramount factors (ref. 2). The available transmission bandwidth was not a limiting factor; however, for the more distant Martian descent mission, the available transmission bandwidth becomes the dominant limitation to securing high-resolution and overlapping pictures. The purpose of this study is to provide an analytical approach to determining transmission rate and camera requirements and also to present some preliminary estimates of these requirements. Basic to this approach is the idea of fixing a proper overlap requirement for successive pictures because wasteful data would be transmitted for a larger overlap, and failure of locating the landing site could result from a smaller overlap. Based on this specification, transmission rate requirements and camera performance, as measured by surface resolution and area coverage, are calculated for three point-mass spacecraft trajectories. These trajectories are the result of numerical integrations of the spacecraft descent motion through two different Martian atmospheric models. These integrations were prepared at the Langley Research Center in support of the Voyager/Mars mission design.

The selected trajectories consist of three phases: ballistic entry, aerodynamic deceleration, and terminal descent. The ballistic-entry phase starts at an altitude of 240 000 meters and terminates with the deployment of a 25-meter parachute at Mach 1.6, which in turn marks the beginning of the aerodynamic decelerator phase. This phase is terminated at an altitude of 1500 meters with the release of the parachute and the activation of a landing propulsion system which reduces vehicle velocity to near zero at the surface.

The final specification of the requirements and prediction of the performance of the imaging system must await the evaluation of at least three other factors: Heat shield ablation due to high vehicle velocities during the ballistic entry phase; vehicle dynamics, especially those caused by the swinging of the parachute during the aerodynamic decelerator phase; and rocket plume obscuration during the terminal descent phase.

#### SYMBOLS

a,b,c	dummy variables
A	area coverage of one frame, <sup>1</sup> square meters
A <sub>0</sub>	area common to two successive image frames, square meters
E	exposure, meter-candle-seconds
f <sub>n</sub>	focal ratio or f-number
F	average value of the two bases of a trapezoid, meters
F <sub>1</sub>	short base of trapezoid, meters (see fig. 6)
F <sub>2</sub>	long base of trapezoid, meters (see fig. 6)
g	phase angle, angle between incident light and camera optical axis, degrees (see fig. 6)
G	altitude of trapezoid, meters (see fig. 6)
H	altitude, meters
H <sub>a</sub>	altitude of orbiter apoapsis, kilometers
H <sub>p</sub>	altitude of orbiter periapsis, kilometers
I	information storage capacity of an image frame, bits
I <sub>0</sub>	information storage capacity inherent in the common area of two overlapping images, bits

j	variable that defines sequence of image frames
K	solar illumination constant at Mars, meter-candles
m	number of binary digits used for encoding shades of grey, bits
n	surface normal
N	number of balanced scan lines per frame, $N = (N_h \times N_v)^{1/2}$
$N_h$	number of elements per line
$N_o$	number of balanced scan lines in the overlapping area of two successive images
$N_v$	number of scan lines
PER	position angle of the spacecraft referenced to the periapsis of the orbiter trajectory, degrees
R	resolution, meters per optical line pair
S	smear, meters
t	time, seconds
$t_E$	exposure time, seconds
$t_p$	time interval between taking pictures, seconds
T	transmission rate, bits per second
v	spacecraft velocity, meters per second
$v_h$	horizontal component of spacecraft velocity, meters per second
$v_v$	vertical component of spacecraft velocity, meters per second
x,y,z	linear distances, meters

$\gamma$	spacecraft flight-path angle, degrees (see fig. 16)
$\epsilon$	angle between optical axis and surface normal, degrees (see fig. 5)
$\zeta$	optical full field of view, degrees
$\iota$	angle between incident illumination and surface normal, degrees (see fig. 6)
$\xi$	angle between spacecraft center line and camera optical axis, degrees (see fig. 16)
$\rho$	normal albedo of Martian surface
$\tau$	white light lens transmission
$\phi$	illumination scattering function

### CONSTRAINTS

The constraints on the imaging experiment which are considered in this study are imposed by the mission objectives, the descent trajectory, the lighting conditions, and the television camera capabilities.

#### Mission-Objectives Constraints

The objectives of this imaging experiment, as described in the introduction, impose three constraints. First, the initial descent picture must be detectable in the orbiter pictures. Second, the successive pictures obtained during descent must overlap in surface coverage in order to establish a continuous chain. Third, the final picture must include the landing site with sufficient resolution, either in the case of a successful soft-landing to relate to the surface-laboratory pictures, or in the case of a landing failure, to detect any surface obstacles which may have caused this failure.

Correlation of the initial descent picture to the orbiter pictures and of successive pictures to each other must be based on image information. The information capacity of an image can be described by considering the image as being sampled in both the vertical and horizontal direction. The total number of independent samples  $N^2$  contained in an image is the product of the number of scan lines  $N_V$  and the number of elements per line  $N_H$ . The parameter  $N$  is frequently referred to as the number of balanced scan lines. If each element is encoded by  $2^m$  shades of grey, then the bits of information that the image frame can contain, at most, are

$$I = mN_h N_v = mN^2 \quad (1)$$

Similarly, the maximum information which can be contained in the overlapping area of two image frames may be given by

$$I_o = mN_o^2 \quad (2)$$

where  $N_o^2$  is the number of elements contained in the common area. Because successive pictures are generally obtained from different altitudes, they have a different number of elements  $N_o^2$  in the area common to each other. (See fig. 1.) Obviously, the lower value is critical and is, therefore, used to specify proper overlap. A required value for  $N_o$  must be based on the amount of detail and contrast contained in the scene to be imaged. In the case of Mars, the pictures obtained from Mariner IV (ref. 3) must serve as guidelines. However, the low contrast obtained in the images, probably due to atmospheric scattering, makes the selection of a required value for  $N_o$  difficult.

For this analysis, the following constraints are assumed:

(a) To correlate the initial descent image to the orbiter pictures, a 200 balanced-line overlap is chosen. Hence, the descent television system must contain at least 200 scan lines, and the area coverage required of the initial pictures depends directly on the surface resolution obtained from the orbiter.

(b) To correlate two successive descent pictures, a 100 balanced-line overlap is chosen.

(c) To correlate the final picture to the surface-laboratory pictures in case of a successful landing or to detect any obstacles which may cause a possible landing failure, a surface resolution of 1 meter per optical line pair is chosen.

The wind speed of storm systems on Mars is believed to average about 50 meters per second and may exceed 100 meters per second (ref. 4). For this reason, the transmission rate required to overlap successive images and image smear are presented for two cases. In one case, no surface wind effects are considered; in the other case, an addition of 60 meters per second to the horizontal spacecraft velocity component is considered.

### Descent Trajectory Constraints

The three descent trajectories used in this study are the result of numerical integrations of the spacecraft motion for two Martian atmospheric models. All the parameters needed to define these trajectories completely are listed in table I. Details on spacecraft trajectory determination and on Martian atmospheric models are presented in reference 5. The trajectory profiles are shown in figure 2. The trajectory parameters

which set the mission constraints are spacecraft altitude, velocity, and flight-path angle and are plotted in figures 3 to 5 as a function of time to impact. Whereas the landing propulsion system will, during the terminal descent phase, reduce the spacecraft velocity to near zero shortly above the surface, in this study the spacecraft is assumed to descend at a constant velocity of 60 meters per second to the surface after parachute release.

### Lighting Constraints

Lighting constraints are imposed on the imaging experiment by the Martian surface reflection characteristics. Exposure of the image sensor is related to these reflection characteristics by the equation (ref. 6)

$$E = K\rho\phi(\epsilon, \iota, g) \frac{\tau E}{4f_n^2} \quad (3)$$

The factors  $K$ ,  $\rho$ , and  $\phi(\epsilon, \iota, g)$  define surface brightness of Mars and the remaining factors define camera characteristics.

Solar illumination of the Martian surface  $K$  during the 1972-73 favorable opposition of Mars is 72 000 meter-candles. The total visible albedo of Mars  $\rho$  is 0.15. This value is an average of many dark and light areas. Measurements of the relative reflectance of dark and light areas observable from the earth indicate albedo values as low as 0.085 and as high as 0.21 (ref. 7). These albedo values may, of course, be averages of still smaller areas, such as will be imaged during this experiment; still wider ranges of albedo values may therefore be encountered.

The illumination scattering function  $\phi(\epsilon, \iota, g)$  accounts for variations in surface brightness and object contrast with changes in lighting and viewing geometry which are shown in figure 6. This function is so normalized that  $\phi(0,0,0) = 1$ . The illumination scattering function for Mars is not well known even after the analysis of Mariner IV pictures (ref. 3). Its apparent similarity with the lunar photometric function (ref. 7) indicates a value of about 0.14 at a phase angle of  $70^\circ$  as a reasonable assumption.

### Television-Camera Constraints

The constraints placed on the parameters of equation (3) by presently available space-qualified television-camera components are those concerning lens f-number  $f_n$ , lens transmission  $\tau$ , and exposure  $E$ .

The illuminance of an image formed by a lens is inversely proportional to the square of the f-number. As shown in figure 7, minimum values of f-numbers currently available for vidicons vary with field of view (ref. 8). This variation occurs since aberrations scale up for the long focal length required for small angular fields and control of the aberrations becomes difficult for large angular fields. Lenses with f-numbers down

to 1.2 are available for fields of view ranging from  $6^\circ$  to  $40^\circ$ . The wide-band visible transmittance of camera lenses ranges from 50 percent to over 80 percent with 70 percent being a good average.

Vidicon sensitivities are such that exposures near 1.0 meter-candle-second produce images of good contrast (ref. 2). Scene brightness changes of two orders of magnitude can be accommodated by incorporating an iris diaphragm. The time interval required for erasing and preparing the photoconductor surface is assumed to equal the read-out time. This interval was, for example, used for the full-scan television system of the Ranger spacecraft (ref. 2).

A nominal value for exposure time of 5 milliseconds is obtained by substituting the quoted values for Martian reflection and television components into equation (3).

## REQUIREMENTS

The requirements for conducting the descent television experiment within the constraints previously outlined can now be estimated. Determined are the number of television systems, their optical field of view, and the transmission rate required to achieve mission objectives.

### Image Resolution and Smear

The area covered by a single image frame, as illustrated in figure 6, is given for a flat surface by

$$A = H^2 \left[ \tan \left( \epsilon + \frac{\xi}{2} \right) - \tan \left( \epsilon - \frac{\xi}{2} \right) \right] \left[ \frac{\tan \frac{\xi}{2}}{\cos \left( \epsilon + \frac{\xi}{2} \right)} + \frac{\tan \frac{\xi}{2}}{\cos \left( \epsilon - \frac{\xi}{2} \right)} \right] \quad (4)$$

One side of the square photoconductor format is assumed to be oriented parallel to the spacecraft flight path. The resulting surface coverage takes the form of a trapezoid for a nonvertical viewing geometry.

The relationships given in this section for geometrical resolution and resolution degradation by smear have been derived and discussed in reference 6. The surface resolution at the center of the frame, sometimes called intrinsic resolution, is

$$R = \frac{2.8H \left( 2 \tan \frac{\xi}{2} \right)}{N \cos^2 \epsilon} \quad (5)$$

The constant 2.8 changes television lines to optical line pairs and includes the Kell factor.

This resolution may be degraded by image smear or blur caused by spacecraft motion during exposure, rocket exhaust plumes, atmospheric turbulence, and lack of focus. Smear due to spacecraft motion can be divided into four components: smear due to translational motion perpendicular to the optical axis (linear smear); smear due to translational motion parallel to the optical axis (zoom effect or edge blur); smear due to camera rotation about an axis perpendicular to the optical axis; and smear due to rotation about the optical axis. Only linear smear and edge blur can result from the point-mass motion of a spacecraft to which this analysis is constrained.

Edge blur appears in the form of points moving radially outward from the center of the frame (for a spacecraft approaching the target). It is zero at the center of the picture and maximum at the edges. Edge blur is, therefore, multidirectional and may tend either to compensate for the linear smear or add to it. Since image smear is most critical at the edge of the image frame where overlap between two successive pictures must be achieved, it is appropriate to use the sum of linear smear and maximum edge blur as given by

$$S = \frac{vt_E \left( \sin \xi + \cos \xi \tan \frac{\xi}{2} \right)}{\cos \epsilon} \quad (6)$$

Resolution degradation due to image smear is perceptible to the human eye if it is equivalent to approximately 0.25 resolution element; this degradation corresponds to  $2.8 \times 0.25 = 0.7$  scan line. An upper boundary can, therefore, be established by requiring that the resolution degradation be less than 0.25 resolution element. Otherwise, a lens of lesser resolution capability but wider field of view would be desirable.

#### Image Transmission Rate

In the absence of a data compression scheme and under the constraint that time to erase and prepare the image surface equal read-out time, the transmission rate required to transmit an image frame containing  $N$  balanced scan lines and a brightness word of  $m$  bits is

$$T = \frac{2mN^2}{t_p} \quad (7)$$

where  $t_p$  is the time interval between taking two pictures. The transmission rate can be halved by employing two identical television systems, which alternately transmit information and erase and prepare their vidicon surfaces.

A general expression for  $t_p$  is derived in the appendix. Considering, for simplicity, only the case where the spacecraft flight-path angle does not change significantly between two successive pictures, as is the case most of the time during spacecraft descent, gives  $t_p$  as

$$t_p = \frac{1}{2a} \left( b - \sqrt{b^2 - 4ac} \right) \quad (8a)$$

providing that the vertical spacecraft velocity component  $v_v \neq 0$ ; if  $v_v = 0$ , then

$$t_p = \frac{c}{b} \quad (8b)$$

where

$$a = v_v \left\{ v_v \left[ \tan \left( \epsilon + \frac{\xi}{2} \right) - \tan \left( \epsilon - \frac{\xi}{2} \right) - 2 \tan \epsilon \right] + 2v_h \right\}$$

$$b = H \left\{ v_v \left[ 3 \tan \left( \epsilon + \frac{\xi}{2} \right) - 3 \tan \left( \epsilon - \frac{\xi}{2} \right) - 2 \tan \epsilon \right] + 2v_h \right\}$$

$$c = 2H^2 \left( 1 - \frac{N_o^2}{N^2} \right) \left[ \tan \left( \epsilon + \frac{\xi}{2} \right) - \tan \left( \epsilon - \frac{\xi}{2} \right) \right]$$

#### Variation of Resolution, Area Coverage, and Transmission Rate With Spacecraft Descent

The variation of surface resolution, area coverage, and required transmission rate with spacecraft descent is now presented. Considered are the three trajectories described earlier, a 200-line television system, a 100 balanced-line overlap ( $N_o = 100$ ), and fields of view ranging from  $4^\circ$  to  $64^\circ$ . An analytical procedure for optimizing the combination of camera field of view and number of balanced scan lines to secure proper overlap between successive pictures and maximum surface resolution for a required transmission rate has been developed in reference 9.

As may be observed from figure 5, the spacecraft angle ( $90^\circ - |\gamma|$ ), discussed in the appendix, remains near  $70^\circ$  to  $80^\circ$  for the larger part of the ballistic entry phase and then changes rapidly to near  $0^\circ$  during the period of parachute deployment. This characteristic, which is common to the three trajectories, suggests that two viewing positions be considered. In one case, the camera optical axis is considered to be pointed away from the spacecraft center line toward the Martian surface during the ballistic entry phase and along the center line after parachute deployment. In the other case, the optical axis is considered to be pointed along the spacecraft center line during all three descent phases. In the first case, near vertical viewing geometry is, therefore, maintained during all three phases of the descent, and in the second case, only during the last two phases.

The variation in surface resolution, area coverage, and transmission rate during the ballistic entry and aerodynamic decelerator phase is given for the first case in

figures 8, 9, and 10, respectively. The discontinuity of the curves is caused by the assumed change in the viewing direction of the camera optical axis with respect to the vehicle center line at the time of parachute deployment. For the second case, the variation in resolution and transmission rate is given in figures 11 and 12. The variation of all three parameters during the final descent phase is given in figure 13.

Resolution degradation due to smear is based on a 5-millisecond exposure time and includes the effect of a 60-meter-per-second surface wind blowing in the direction of the horizontal spacecraft velocity component. The transmission rate required to overlap successive images is given for both the absence and presence of this wind.

Area coverage during ballistic entry for the second case, where the camera optical axis is considered to be pointed along the spacecraft center line, is not given because the curvature of the planet becomes significant for fields of view above  $16^\circ$ , whereas the equations used in this study are based on a flat surface. For the same reason, the transmission rate required during ballistic entry is given in figure 12 only for fields of view of  $16^\circ$  and less. For both cases, the transmission rate is also not given near parachute deployment because the spacecraft flight-path angle changes rapidly during this period, and the equation used for calculating transmission rate is limited to the condition that viewing geometry does not change significantly during the interval between two successive exposures.

### Discussion of Results

Although the effect of a 60-meter-per-second surface wind on the imaging experiment is presented in figures 8 to 13 for all three descent phases, its effect is very likely negligible except during the aerodynamic decelerator phase. Only the large frontal area of a parachute can be expected to respond significantly to the low dynamic pressures prevailing on Mars. In the following discussion, the effect of surface wind is, therefore, considered only for this phase.

To facilitate the selection of the field of view and transmission rate required for a 200-line television system to accomplish the specified mission objectives, all pertinent information is summarized in tables II to IV. These tables present the transmission rate required to overlap successive pictures for various fields of view during each descent phase. In addition, table IV provides also the transmission rate required to transmit before touchdown an image of the landing site with a surface resolution of 1 meter per optical-line pair.

Figure 14 illustrates how the information compiled in tables II to IV may be used to select the field of view which minimizes the transmission rate required for conducting the experiment with a 200-line television system. Considered in this plot are the trajectory A, the effect of the surface wind during the aerodynamic decelerator phase, and

near vertical viewing geometry during ballistic entry. The plot reveals a minimum required transmission rate of  $1.6 \times 10^5$  bits per second for a field of view of  $14^\circ$ . A narrower field of view would require a higher transmission rate during the ballistic entry phase, and a wider field of view would require a higher transmission rate during the terminal descent phase. It may be recalled that image information was assumed to be transmitted directly as it was scanned off the photoconductor surface and that the photoconductor erase-and-prepare time was assumed to equal the read-out time. In this case, the time interval allowed for the photoconductor erase-and-prepare mode would be

$$\frac{mN^2}{T} = \frac{6 \times (200)^2 \text{ bits per image}}{1.6 \times 10^5 \text{ bits per second}} = 1.5 \text{ seconds per image}$$

As mentioned before, two television systems employed alternately for transmitting image information would halve the required transmission rate, in this case to  $8 \times 10^4$  bits per second, and double the allowed time interval for the erase-and-prepare mode, in this case to 3 seconds per image.

Results for several other cases are summarized in table V. In all cases, the effect of the surface wind is considered only during the aerodynamic decelerator phase. If the effect of the surface wind is also considered during the terminal descent phase, the requirements resulting from this phase would dominate all others regardless of the field of view. The minimum required transmission rate would then be  $8.4 \times 10^5$  bits per second (for a single television system).

As indicated in table V, the viewing geometry employed during the ballistic-entry phase influences the required transmission rate. If the camera optical axis is pointed along the spacecraft center line rather than along the surface normal, the optimum field of view is  $12^\circ$  and the required transmission rate is  $1.4 \times 10^5$  bits per second for all three trajectories. If the optical axis is pointed normal to the surface, then the optimum fields of view widen to  $14^\circ$ ,  $20^\circ$ , and  $22^\circ$  and the required transmission rates increase to  $1.6 \times 10^5$ ,  $2.4 \times 10^5$ , and  $2.7 \times 10^5$  bits per second for trajectories A, B, and C, respectively. However, as can be observed by comparing figures 8 and 11, this increase in transmission rate produces a better surface resolution during some periods of the ballistic entry phase by more than a factor of 10.

One constraint imposed on the television experiment by the mission objectives, namely the correlation of the initial-descent picture to the pictures obtained from an orbiter, has not yet been discussed. As mentioned before, the area coverage required of the initial-descent picture depends directly on the resolution of the orbiter pictures. The initial area coverage, in turn, allows the selection of spacecraft altitude and camera field of view required for the first picture directly from figure 9. Depending on the descent trajectory or, more specifically, the altitude of parachute deployment, the surface

resolution obtained from an orbiter may decide, therefore, whether the television experiment must be initiated during the ballistic-entry phase or may be allowed to start after parachute deployment. Initiation of this experiment after parachute deployment could simplify the implementation of the television system considerably.

## CONCLUSIONS

An analytical study was made to present a systematic approach towards determining the transmission rate and field-of-view requirements of a television experiment on board a spacecraft as it descends through the Martian atmosphere. From consideration of the image information common to two successive pictures as the proper criteria for specifying image overlap, an expression was derived for the transmission rate required to secure this overlap as a function of point-mass trajectory values and television camera characteristics. Variations of this transmission rate and of surface resolution and coverage was calculated and plotted as a function of three spacecraft descent trajectories. A 200 balanced-scan-line television was selected for these calculations as a compromise between desirable surface resolution and transmission-rate requirement, and a 100-line overlap between successive pictures was assumed sufficient to secure a continuous image chain.

Results show that a single television system can provide a chain of overlapping pictures and a final surface resolution of 1 meter per optical line pair. The required transmission rates range from  $1.4 \times 10^5$  to  $2.7 \times 10^5$  bits per second and the fields of view from  $12^\circ$  to  $22^\circ$ , depending on the descent trajectory and the camera viewing direction. The possible adverse effect of a steady 60-meter-per-second surface wind during the parachute descent phase is included. If the vidicon erase-and-prepare time is made equal to the read-out time, then the required transmission rate may be halved by employing two television systems. Whether the television experiment must be initiated during the ballistic entry phase or can be allowed to start after parachute deployment depends on the surface resolution provided by the orbiter pictures and the altitude of parachute deployment.

Langley Research Center,  
National Aeronautics and Space Administration,  
Langley Station, Hampton, Va., November 22, 1968,  
125-24-01-11-23.

## APPENDIX

### DERIVATION OF THE TIME INTERVAL BETWEEN EXPOSURES FOR SECURING A REQUIRED OVERLAP BETWEEN SUCCESSIVE PICTURES

This appendix presents the derivation of an expression for the maximum time interval which may be allowed between exposures for securing proper overlap between the successive pictures obtained from a moving spacecraft. The derivation was first presented in reference 9 and is repeated herein because of its significance to the basic approach taken in this paper as well as to the final results.

Viewing geometry and surface coverage are shown in figure 6. One side of the square photoconductor format is assumed to be parallel to the spacecraft flight path. The resulting surface coverage takes the form of a trapezoid for a nonvertical viewing geometry. To simplify the derivation, this trapezoid is approximated by a rectangle. In this approximation, the altitude of the trapezoid  $G$  becomes the length of the rectangle along the direction of the spacecraft flight path, and the average of the two bases of the trapezoid  $F_1$  and  $F_2$  becomes the width of the rectangle perpendicular to the flight path. This average width is given by  $F = \frac{1}{2}(F_1 + F_2)$ . It may be noted that the total surface coverage has not been changed by this approximation.

As indicated in figure 1, two successive images must share a certain amount of surface information in order that these images may be matched. Each image has an information storage capacity given by  $I = mN^2$ .

The information storage capacity of the surface area  $A_0$  common to both images due to picture  $j$  is

$$I_{O,j} = \frac{mN^2 A_0}{A_j} \quad (A1)$$

and due to picture  $j + 1$  is

$$I_{O,j+1} = \frac{mN^2 A_0}{A_{j+1}} \quad (A2)$$

For a descending spacecraft,  $A_j \geq A_{j+1}$  and therefore  $I_{O,j} \leq I_{O,j+1}$ . Since the lower value of information about the surface area common to two successive images is critical, the overlap requirement is specified by  $I_{O,j} = I_0$ . By referring to figure 15, equation (A1) may be rewritten in the form

$$\frac{x_{j,j+1} F_{j+1}}{F_j G_j} = \frac{N_0^2}{N^2} \quad (A3)$$

where  $N_0^2$  is the number of scan elements contained in the area  $A_0$  due to picture  $j$ .

## APPENDIX

The dimension  $y_{j,j+1}$  as obtained from figure 15 is

$$y_{j,j+1} = \frac{1}{2}(G_j + G_{j+1}) - x_{j,j+1} \quad (\text{A4})$$

and as obtained from figure 16 is

$$y_{j,j+1} = z_{j,j+1} - H_j \tan \epsilon_j + H_{j+1} \tan \epsilon_{j+1} \quad (\text{A5})$$

Equating the right side of equations (A4) and (A5), and substituting for  $x_{j,j+1}$  by the expression given in equation (A3) yields

$$z_{j,j+1} - H_j \tan \epsilon_j + H_{j+1} \tan \epsilon_{j+1} = \frac{1}{2}(G_j + G_{j+1}) - \frac{N_o^2}{N^2} \frac{F_j G_j}{F_{j+1}} \quad (\text{A6})$$

By using the viewing geometry shown in figure 6 and the approximation  $F = \frac{1}{2}(F_1 + F_2)$ , the dimensions of picture coverage are given as

$$F_j = H_j \left[ \frac{\tan \frac{\zeta}{2}}{\cos \left( \epsilon_j - \frac{\zeta}{2} \right)} + \frac{\tan \frac{\zeta}{2}}{\cos \left( \epsilon_j + \frac{\zeta}{2} \right)} \right] \quad (\text{A7})$$

$$G_j = H_j \left[ \tan \left( \epsilon_j + \frac{\zeta}{2} \right) - \tan \left( \epsilon_j - \frac{\zeta}{2} \right) \right] \quad (\text{A8})$$

$$F_{j+1} = H_{j+1} \left[ \frac{\tan \frac{\zeta}{2}}{\cos \left( \epsilon_{j+1} - \frac{\zeta}{2} \right)} + \frac{\tan \frac{\zeta}{2}}{\cos \left( \epsilon_{j+1} + \frac{\zeta}{2} \right)} \right] \quad (\text{A9})$$

$$G_{j+1} = H_{j+1} \left[ \tan \left( \epsilon_{j+1} + \frac{\zeta}{2} \right) - \tan \left( \epsilon_{j+1} - \frac{\zeta}{2} \right) \right] \quad (\text{A10})$$

It is convenient to define the time interval between the exposure of two successive images as  $t_p = |t_j - t_{j+1}|$  and the average horizontal spacecraft velocity component during that time as

$$\langle v_h \rangle \equiv \langle v_h \rangle_{j,j+1} = \frac{1}{t_p} \int_{t_j}^{t_{j+1}} v(t) \cos \gamma(t) dt \quad (\text{A11})$$

and, similarly, the average vertical velocity component as

$$\langle v_v \rangle \equiv \langle v_v \rangle_{j,j+1} = \frac{1}{t_p} \int_{t_j}^{t_{j+1}} v(t) \sin \gamma(t) dt \quad (\text{A12})$$

## APPENDIX

By using these definitions, the parameter  $z_{j,j+1}$  can be written as

$$z_{j,j+1} = \langle v_h \rangle t_p \quad (\text{A13})$$

and the altitudes  $H_j$  and  $H_{j+1}$  are related by

$$H_{j+1} = H_j - \langle v_v \rangle t_p \quad (\text{A14})$$

An expression for  $t_p$  is derived by substituting equations (A13) and (A14) into equation (A6) as follows:

$$\begin{aligned} & \langle v_h \rangle t_p - H_j \tan \epsilon_j + H_j \tan \epsilon_{j+1} - \langle v_v \rangle t_p \tan \epsilon_{j+1} \\ &= \frac{1}{2} \left( \frac{G_j}{H_j} \right) H_j + \frac{1}{2} \left( \frac{G_{j+1}}{H_{j+1}} \right) (H_j - \langle v_v \rangle t_p) - \frac{N_o^2}{N^2} \frac{\left( \frac{F_j}{H_j} \right) \left( \frac{G_j}{H_j} \right) H_j^2}{\left( \frac{F_{j+1}}{H_{j+1}} \right) (H_j - \langle v_v \rangle t_p)} \end{aligned} \quad (\text{A15})$$

The ratios  $F_j/H_j$ ,  $G_j/H_j$ ,  $F_{j+1}/H_{j+1}$ , and  $G_{j+1}/H_{j+1}$  can be obtained from equations (A7) to (A10). These ratios are independent of velocity and altitude and dependent only on the viewing geometry of pictures  $j$  and  $j+1$ . Solving equation (A15) for  $t_p$  yields a quadratic equation which has the solution

$$t_p = \frac{1}{2a} \left( b - \sqrt{b^2 - 4ac} \right) \quad (\text{A16a})$$

providing that  $\langle v_v \rangle \neq 0$ ; if  $\langle v_v \rangle = 0$ , then

$$t_p = \frac{c}{b} \quad (\text{A16b})$$

where

$$\begin{aligned} a &= \langle v_v \rangle \left\{ \langle v_v \rangle \left[ \frac{1}{2} \left( \frac{G_{j+1}}{H_{j+1}} \right) - \tan \epsilon_{j+1} \right] + \langle v_h \rangle \right\} \\ b &= H_j \left\{ \langle v_v \rangle \left[ \frac{1}{2} \left( \frac{G_j}{H_j} \right) + \frac{G_{j+1}}{H_{j+1}} + \tan \epsilon_j - 2 \tan \epsilon_{j+1} \right] + \langle v_h \rangle \right\} \\ c &= H_j^2 \left[ \frac{1}{2} \left( \frac{G_j}{H_j} \right) + \frac{1}{2} \left( \frac{G_{j+1}}{H_{j+1}} \right) + \tan \epsilon_j - \tan \epsilon_{j+1} - \frac{N_o^2}{N^2} \frac{\left( \frac{F_j}{H_j} \right) \left( \frac{G_j}{H_j} \right)}{\left( \frac{F_{j+1}}{H_{j+1}} \right)} \right] \end{aligned}$$

## APPENDIX

For portions of the trajectory where the viewing geometry and spacecraft velocity change only insignificantly during the time interval  $t_p$ , that is, where  $\epsilon_j \approx \epsilon_{j+1}$  and  $\langle v \rangle_{j,j+1} \approx v_{j+1} \approx v_j$ , the parameters a, b, and c of equations (A16) can be approximated by a simple expression. In this approximation

$$\frac{F_j}{H_j} = \frac{F_{j+1}}{H_{j+1}} = \frac{\tan \frac{\xi}{2}}{\cos \left( \epsilon_j - \frac{\xi}{2} \right)} + \frac{\tan \frac{\xi}{2}}{\cos \left( \epsilon_j + \frac{\xi}{2} \right)} \quad (\text{A17})$$

and

$$\frac{G_j}{H_j} = \frac{G_{j+1}}{H_{j+1}} = \tan \left( \epsilon_j + \frac{\xi}{2} \right) - \tan \left( \epsilon_j - \frac{\xi}{2} \right) \quad (\text{A18})$$

Substituting equations (A17) and (A18) into expressions for a, b, and c of equations (A16) yields

$$\begin{aligned} a &= v_{v,j} \left\{ v_{v,j} \left[ \tan \left( \epsilon_j + \frac{\xi}{2} \right) - \tan \left( \epsilon_j - \frac{\xi}{2} \right) - 2 \tan \epsilon_j \right] + 2v_{h,j} \right\} \\ b &= H_j \left\{ v_{v,j} \left[ 3 \tan \left( \epsilon_j + \frac{\xi}{2} \right) - 3 \tan \left( \epsilon_j - \frac{\xi}{2} \right) - 2 \tan \epsilon_j \right] + 2v_{h,j} \right\} \\ c &= 2H_j^2 \left( 1 - \frac{N_o^2}{N^2} \right) \left[ \tan \left( \epsilon_j + \frac{\xi}{2} \right) - \tan \left( \epsilon_j - \frac{\xi}{2} \right) \right] \end{aligned}$$

## REFERENCES

1. Spradley, L. Harold; Steinbacher, R.; Grolier, M.; and Byrne, C.: Surveyor I: Location and Identification. *Science*, vol. 157, no. 3789, Aug. 11, 1967, pp. 681-684.
2. Kindt, Donald H.; and Staniszewski, Joseph R.: The Design of the Ranger Television System To Obtain High-Resolution Photographs of the Lunar Surface. Tech. Rep. No. 32-717 (Contract No. NAS 7-100), Jet Propulsion Lab., California Inst. Technol., Mar. 1, 1965, pp. 8-13.
3. Leighton, Robert B.; Murray, Bruce C.; Sharp, Robert P.; Allen, J. Denton; and Sloan, Richard K.: Mariner Mars 1964 Project Report: Television Experiment. Part I. Investigators' Report. Tech. Rep. No. 32-884 (Contract No. NAS 7-100), Jet Propulsion Lab., California Inst. Technol., Dec. 15, 1967.
4. Evans, Dallas E.; Pitts, David E.; and Kraus, Gary L.: Venus and Mars Nominal Natural Environment for Advanced Manned Planetary Mission Programs. Second ed.. NASA SP-3016, 1967, p. 36.
5. Anon.: Comparative Studies of Conceptual Design and Qualification Procedures for a Mars Probe/Lander. Volume V: Subsystem and Technical Analysis - Book 1: Trajectory Analysis. AVSSD-0006-66-RR (Contract NAS 1-5224), AVCO Corp., May 11, 1966.
6. Herriman, A. G.; Washburn, H. W.; and Willingham, D. E.: Ranger Preflight Science Analysis and the Lunar Photometric Model. Tech. Rep. No. 32-384 (Rev.) (Contract No. NAS 7-100), Jet Propulsion Lab., California Inst. Technol., Mar. 11, 1963.
7. Harris, Daniel L.: Photometry and Colorimetry of Planets and Satellites. *Planets and Satellites*, Gerard P. Kuiper and Barbara M. Middlehurst, eds., Univ. of Chicago Press, c.1961, pp. 272-342.
8. Tuttle, Clifton M., ed.: The Optical Industry and Systems Directory. The Optical Pub. Co., Inc., c.1966, pp. 331-354.
9. Huck, Friedrich O.: An Analytical Procedure for Optimizing Television Systems for Planetary Descent Missions. NASA TN D-5061, 1969.

TABLE I.- SUMMARY OF DESCENT TRAJECTORY PARAMETERS

[From ref. 5]

	Trajectory A	Trajectory B	Trajectory C
Atmospheric model . . . . .	VM-3 (10 mb)	VM-8 (5 mb)	VM-8 (5 mb)
Orbiter trajectory:			
H <sub>p</sub> , km . . . . .	1100	1000	1000
H <sub>a</sub> , km . . . . .	10 000	20 000	20 000
True anomaly at de-orbit, deg . . . . .	220	250	240
Flight-path angle at 240 000 meters, deg . . . . .	19.8	14.5	20
Landing PER:			
Vacuum, deg . . . . .	-28.5	3.5	-18.6
Atmosphere, deg . . . . .	-30.3	0	-19.5
Ballistic coefficient:			
Without parachute . . . . .	0.25	0.25	0.345
With parachute . . . . .	0.034	0.034	0.047

TABLE II.- TRANSMISSION RATE REQUIREMENTS DURING  
BALLISTIC ENTRY PHASE

Orientation of optical axis	Field of view, deg	Transmission rate required to overlap successive pictures for three trajectories, bits/sec		
		A	B	C
Approximately along surface normal	4	$5.2 \times 10^5$	$1.2 \times 10^6$	$1.5 \times 10^6$
	8	$2.6 \times 10^5$	$6.1 \times 10^5$	$7.5 \times 10^5$
	16	$1.4 \times 10^5$	$3.1 \times 10^5$	$3.8 \times 10^5$
	32	$7.1 \times 10^4$	$1.6 \times 10^5$	$2.0 \times 10^5$
	64	$3.7 \times 10^4$	$7.5 \times 10^4$	$1.0 \times 10^5$
Along spacecraft center line	4	$1.3 \times 10^4$	$1.3 \times 10^4$	$3.5 \times 10^4$
	8	$1.3 \times 10^4$	$1.3 \times 10^4$	$3.4 \times 10^4$
	16	$1.3 \times 10^4$	$1.3 \times 10^4$	$3.4 \times 10^4$

TABLE III.- TRANSMISSION RATE REQUIREMENTS DURING  
AERODYNAMIC DECELERATOR PHASE

Field of view, deg	Transmission rate required to:	
	Overlap successive pictures in absence of surface wind, bits/sec	Overlap successive pictures in presence of 60-m/sec surface wind, bits/sec
4	$3.2 \times 10^4$	$3.9 \times 10^5$
8	$3.2 \times 10^4$	$2.0 \times 10^5$
16	$3.2 \times 10^4$	$1.1 \times 10^5$
32	$3.2 \times 10^4$	$6.6 \times 10^4$
64	$3.2 \times 10^4$	$4.4 \times 10^4$

TABLE IV.- TRANSMISSION RATE REQUIREMENTS  
DURING TERMINAL DESCENT PHASE

Field of view, deg	Transmission rate, bits/sec, required to:			
	Transmit a picture with a resolution of 1 meter* before touchdown		Overlap successive pictures	
	In absence of surface wind	In presence of 60-m/sec surface wind	In absence of surface wind	In presence of 60-m/sec surface wind
4	$1.4 \times 10^4$	$2.1 \times 10^4$	$4.5 \times 10^4$	$8.4 \times 10^5$
8	$2.9 \times 10^4$	$4.2 \times 10^4$	$9.2 \times 10^4$	$8.8 \times 10^5$
16	$6.0 \times 10^4$	$8.8 \times 10^4$	$1.9 \times 10^5$	$1.0 \times 10^6$
32	$1.3 \times 10^5$	$2.0 \times 10^5$	$4.2 \times 10^5$	$1.4 \times 10^6$
64	$3.2 \times 10^5$	$5.4 \times 10^5$	$1.0 \times 10^6$	$2.5 \times 10^6$

\*This resolution value includes degradation by smear. In the absence of surface wind, smear is below the acceptable level; in the presence of a 60-m/sec surface wind, smear is above the acceptable level.

**TABLE V.- REQUIREMENTS FOR A 200-LINE TELEVISION SYSTEM  
TO ACCOMPLISH MISSION OBJECTIVES<sup>a</sup>**

Viewing geometry	Trajectory	Field of view, deg	Transmission rate, bits/sec (b)	Erase-and-prepare time, sec (c)
Approximately along surface normal	A	14	$1.6 \times 10^5$	1.5
	B	20	$2.4 \times 10^5$	1.0
	C	22	$2.7 \times 10^5$	0.9
Along spacecraft center line	A, B, C	12	$1.4 \times 10^5$	1.7

<sup>a</sup>The effect of a 60-m/sec surface wind is included only during the aerodynamic decelerator phase.

<sup>b</sup>This transmission rate is given for one television system; it may be halved for two systems.

<sup>c</sup>This time interval is given for one television system; it may be doubled for two systems.

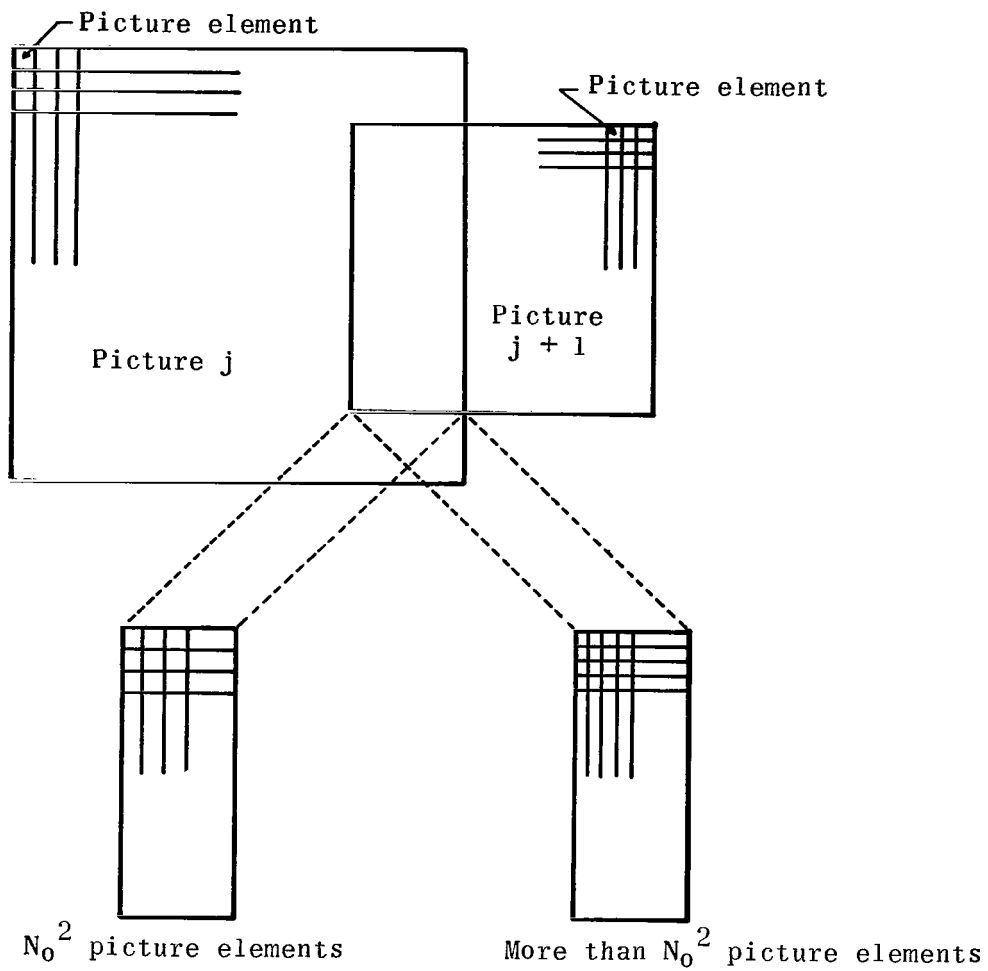


Figure 1.- Footprint of two successive pictures to illustrate proper surface overlap.

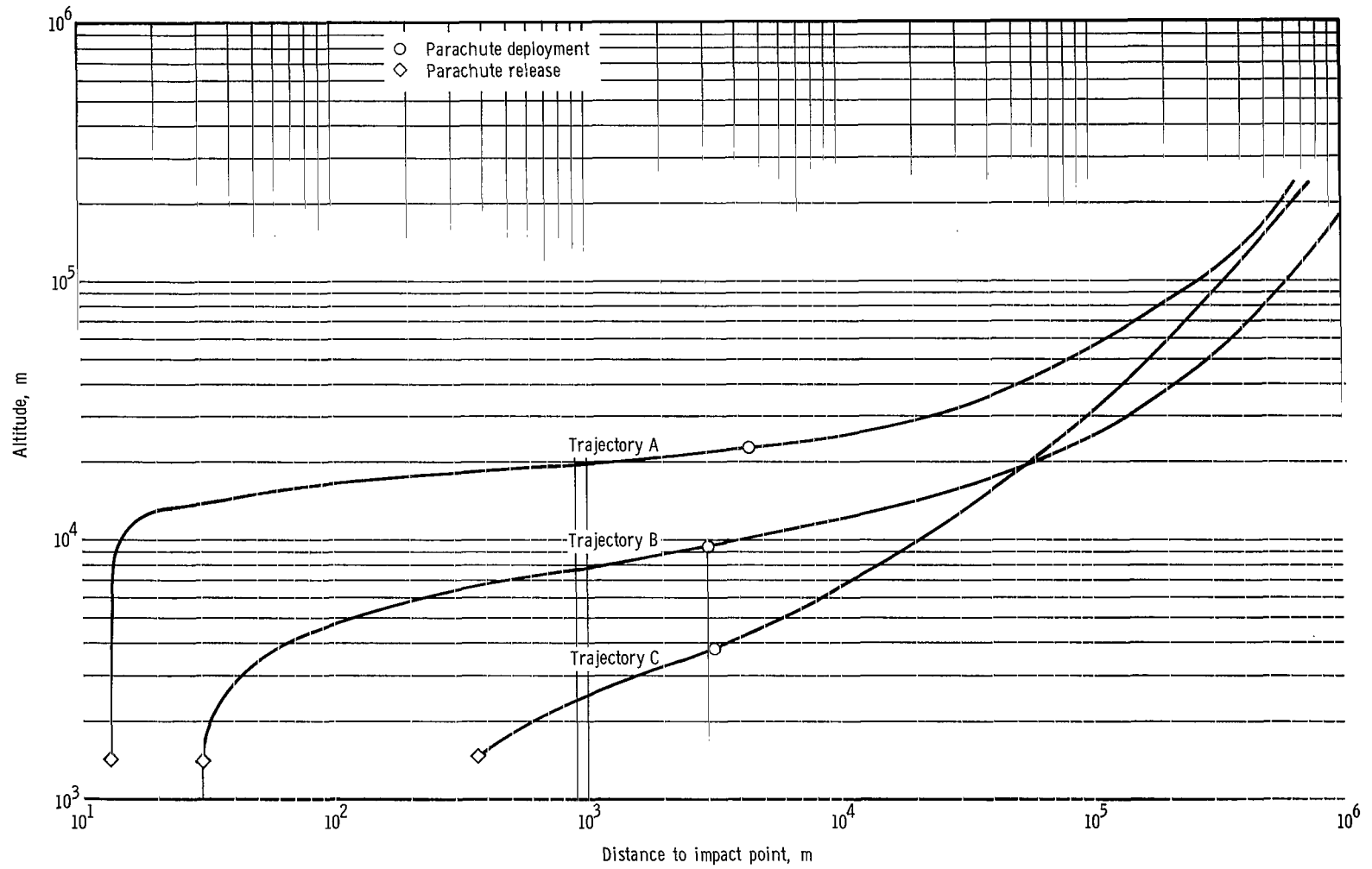


Figure 2.- Profiles of three descent trajectories.

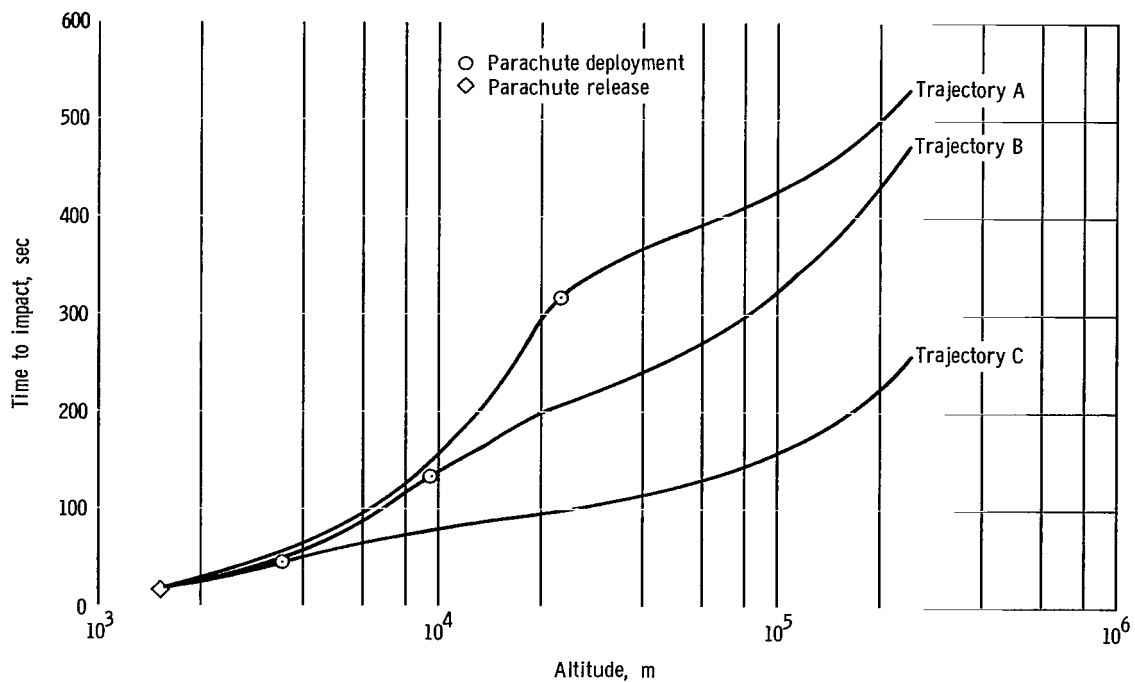


Figure 3.- Variation of altitude with time to impact for three descent trajectories.

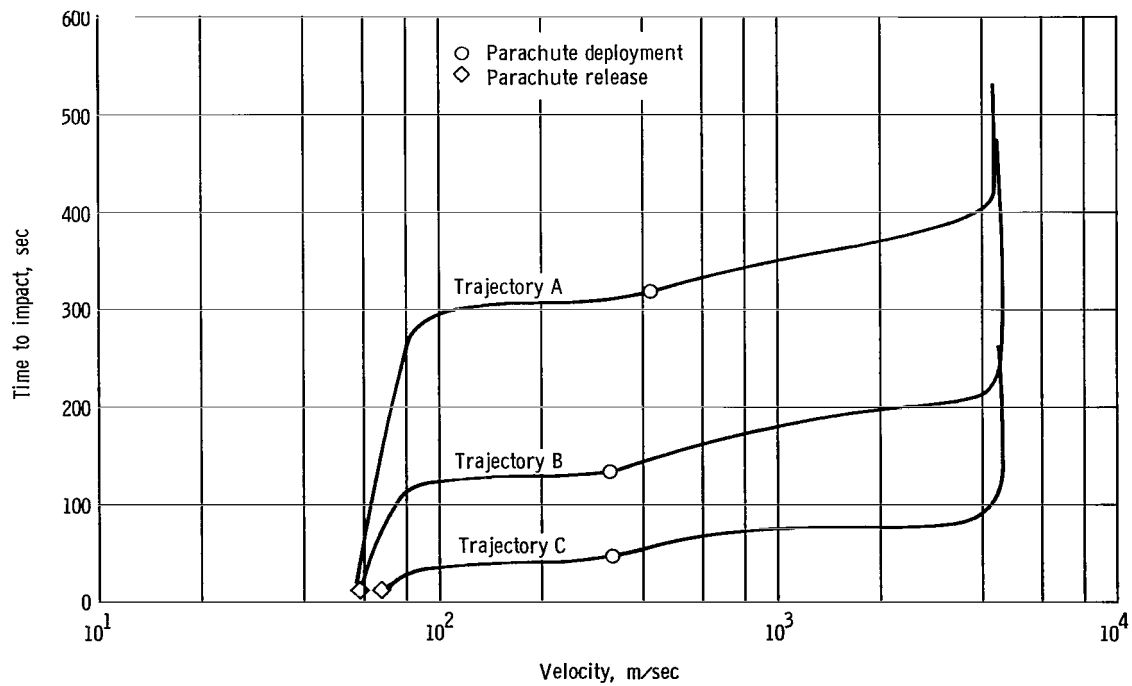


Figure 4.- Variation of velocity with time to impact for three descent trajectories.

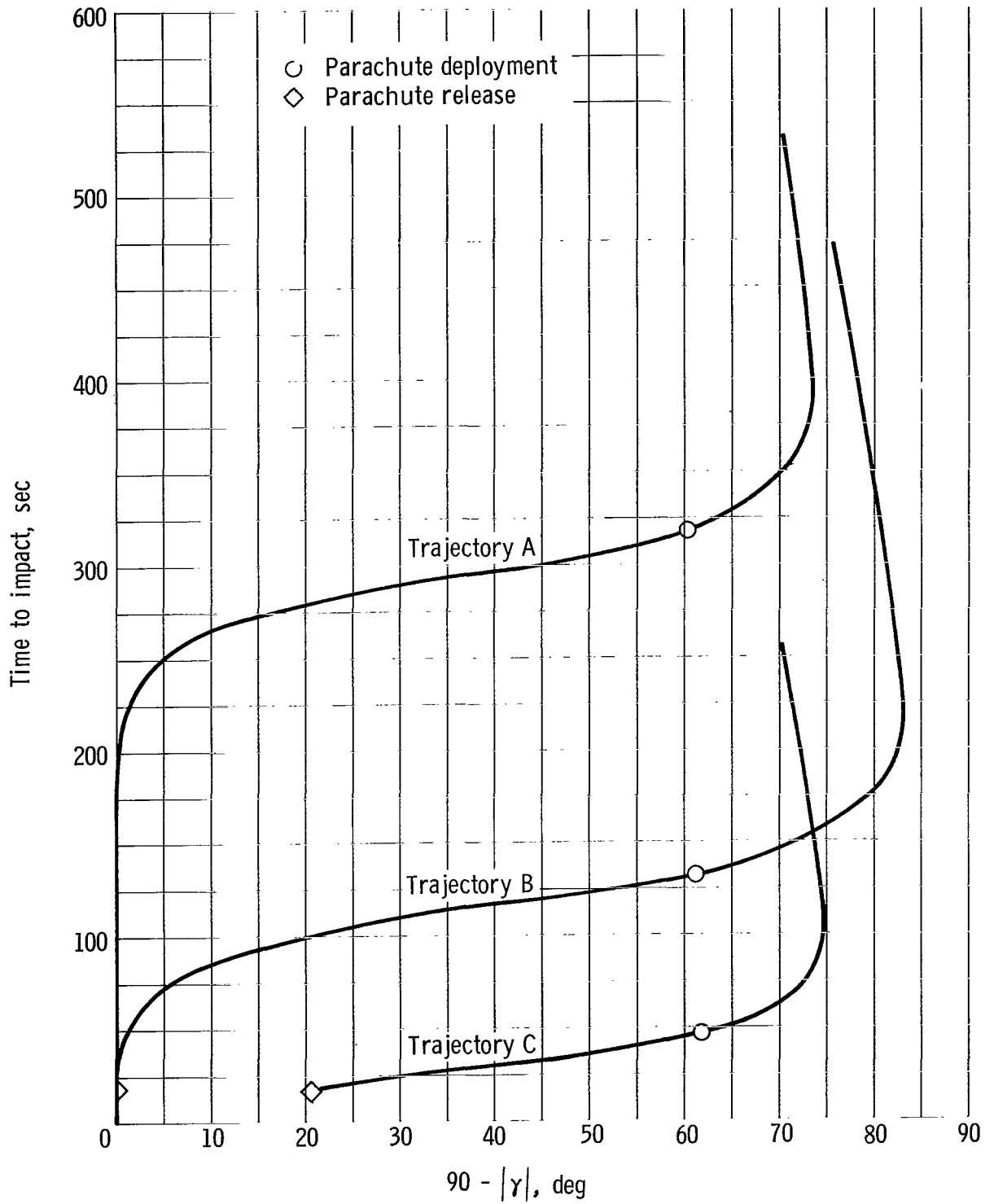


Figure 5.- Variation of flight-path angle with time to impact for three trajectories.

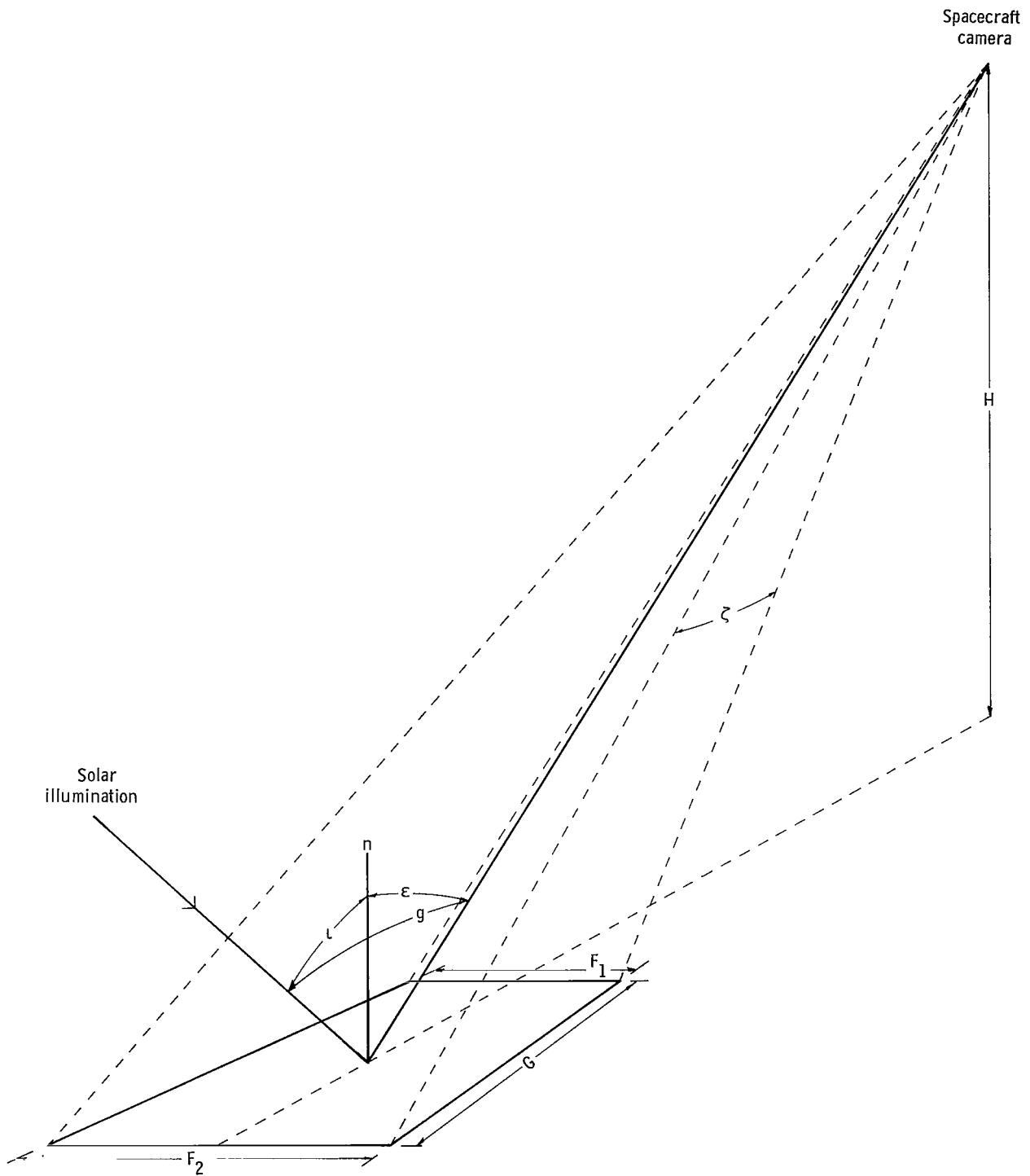


Figure 6.- Illustration of viewing geometry.

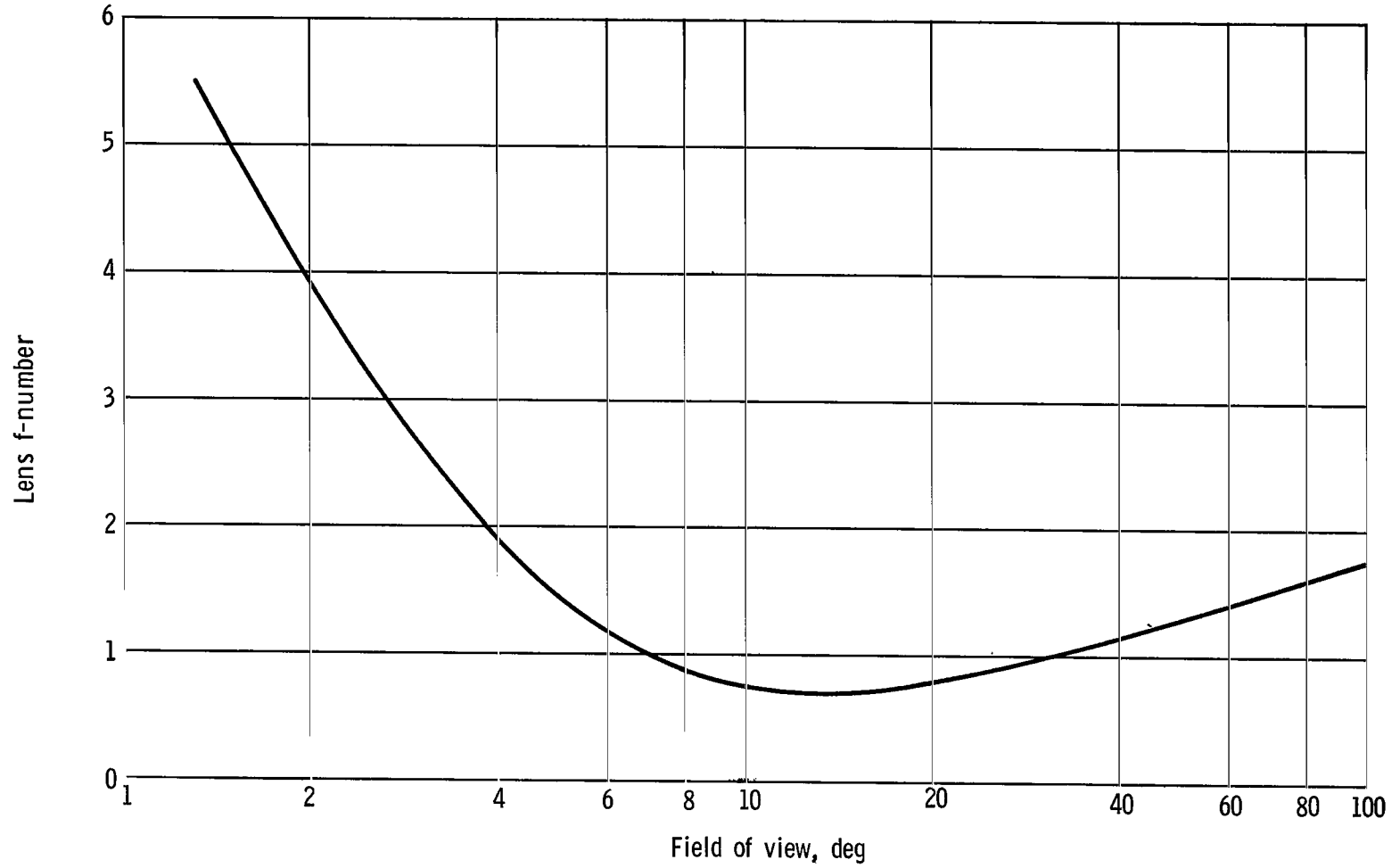


Figure 7.- Variation of lower limit of f-number for commercially available vidicon lenses with field of view. (11.2 × 11.2 mm vidicon format.)

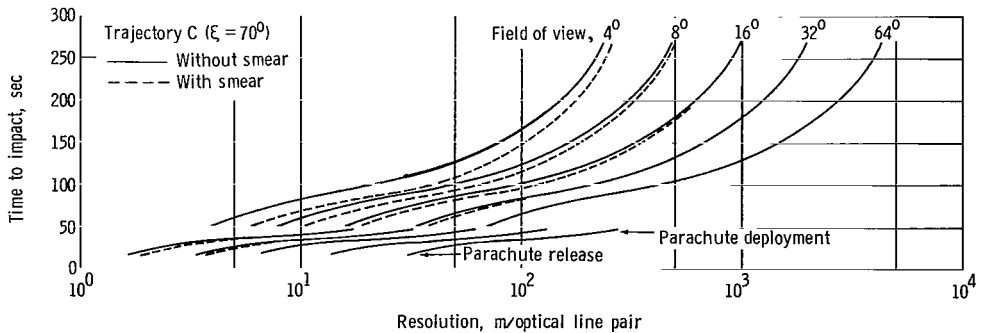
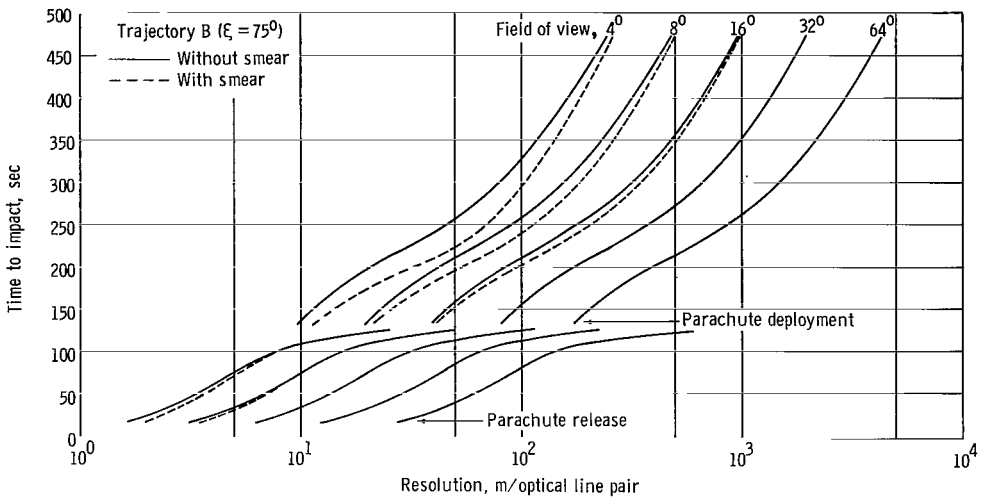
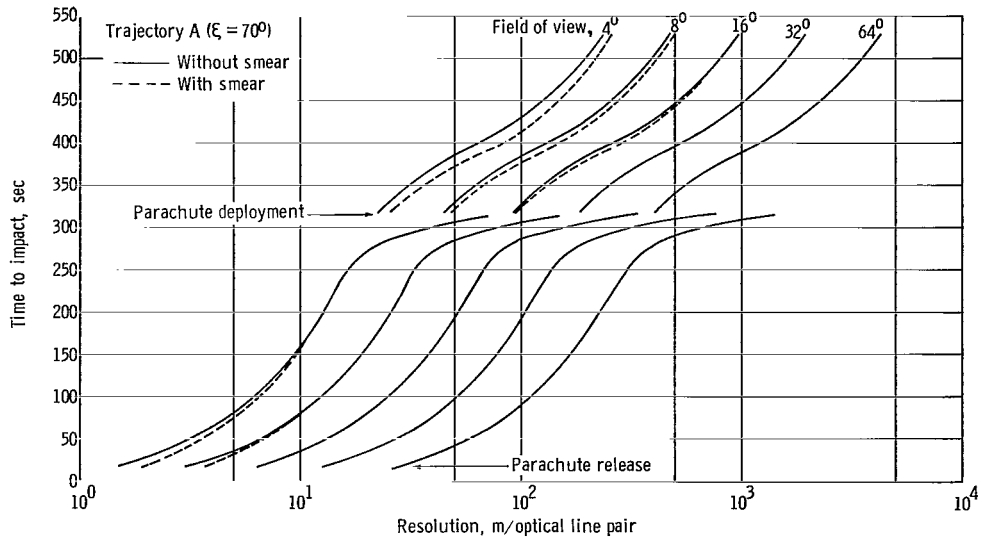


Figure 8.- Variation of surface resolution with time to impact for three descent trajectories. A 200-line television system and several lens field-of-view values are assumed. The television optical axis is turned  $\xi$  degrees from the spacecraft center line toward the Martian surface during the ballistic entry phase and is aligned with the center line during the aerodynamic decelerator phase. Smear is given for an exposure time of 5 msec and includes the effect of a 60-m/sec surface wind blowing in the direction of the flight path.

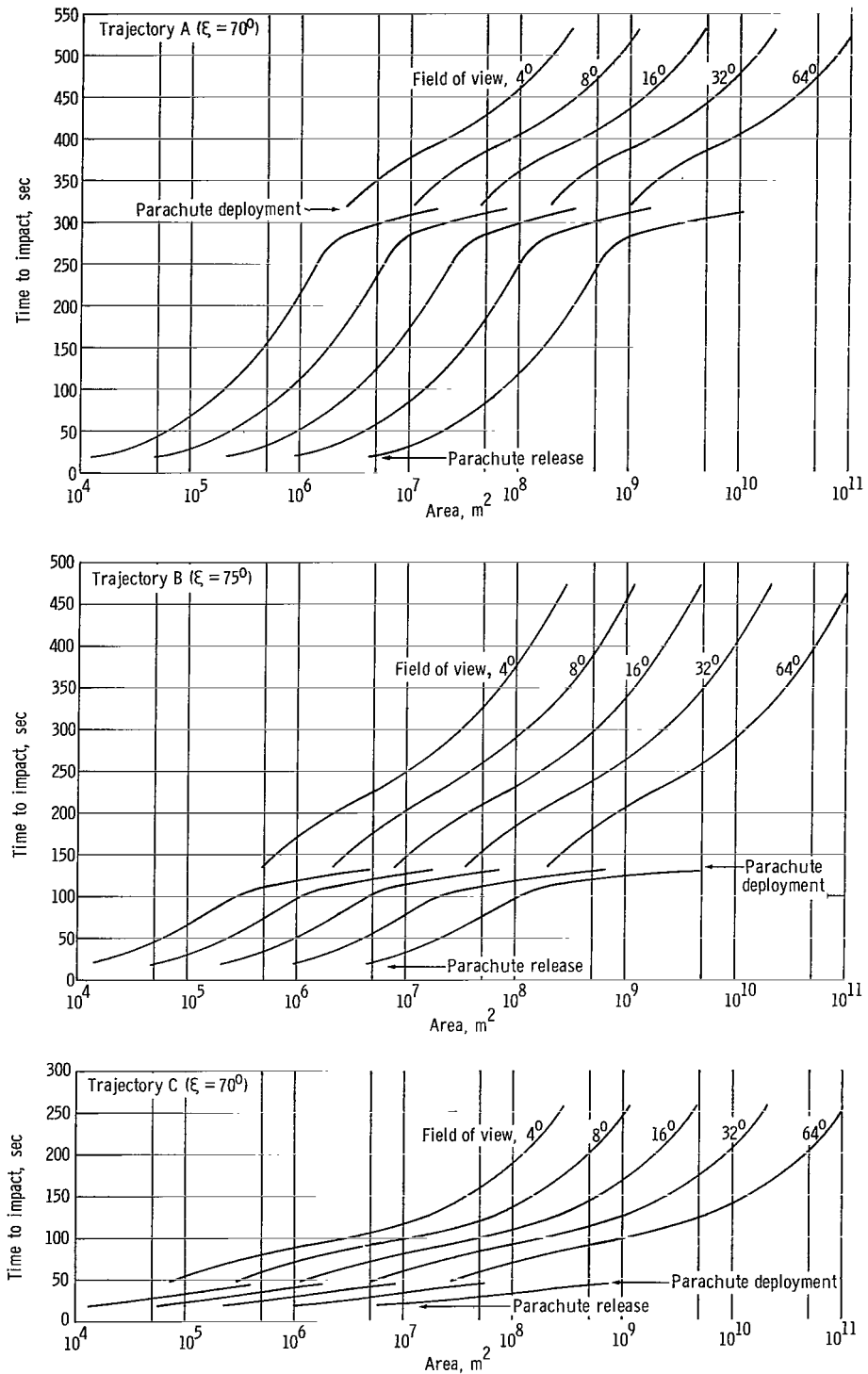


Figure 9.- Variation of area coverage with time to impact for three descent trajectories. Several lens field-of-view values are assumed. The television optical axis is turned  $\xi$  degrees from the spacecraft center line toward the Martian surface during the ballistic entry phase and is aligned with the center line during the aerodynamic decelerator phase.

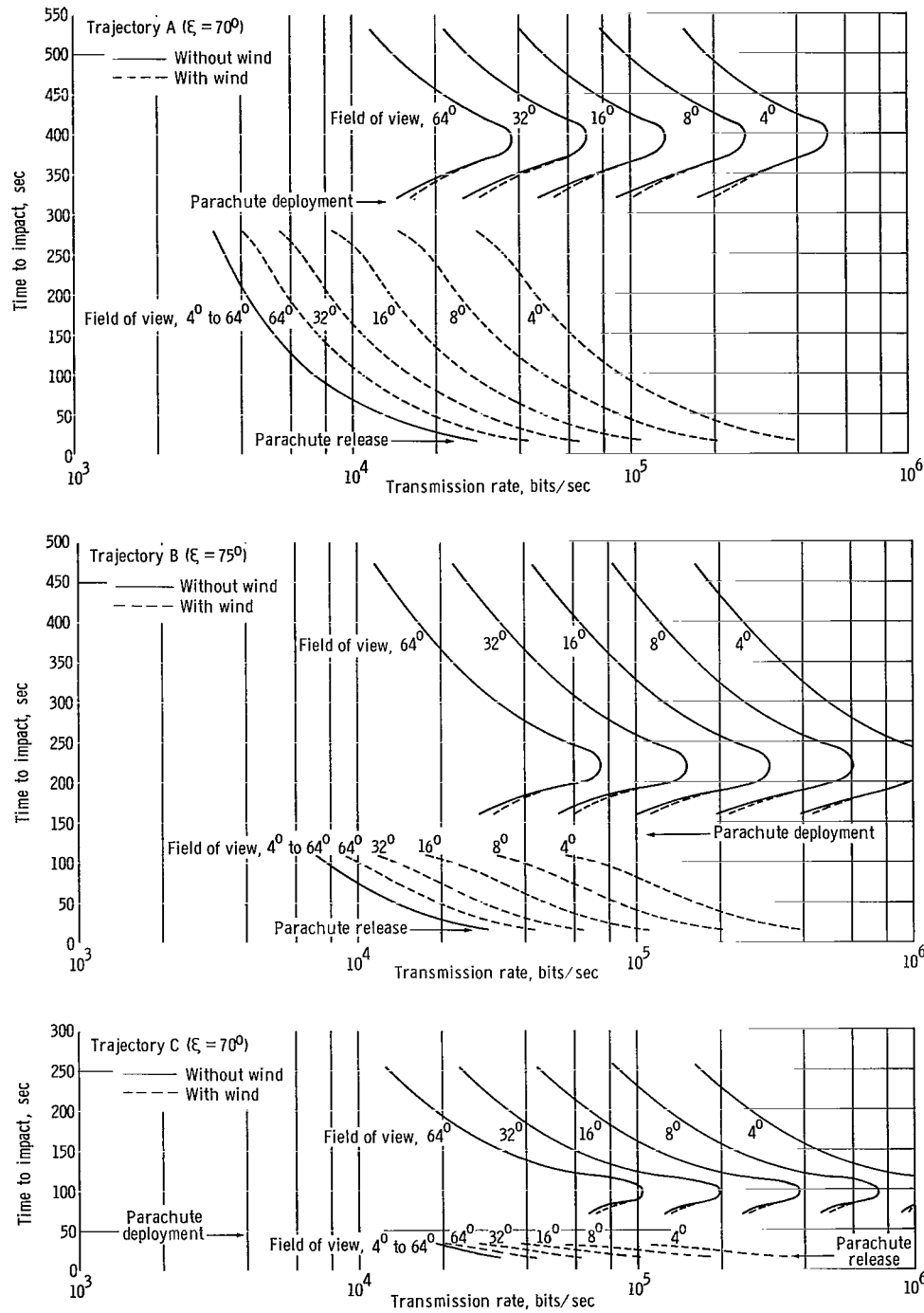


Figure 10.- Variation of transmission rate to achieve overlap of successive pictures with time to impact for three descent trajectories. A 200-line television system and several lens field-of-view values are assumed. The television optical axis is turned  $\xi$  degrees from the spacecraft center line toward the Martian surface during the ballistic entry phase and is aligned with the center line during the aerodynamic decelerator phase. Transmission rate is given for the absence and presence of a 60-m/sec surface wind blowing in the direction of the flight path.

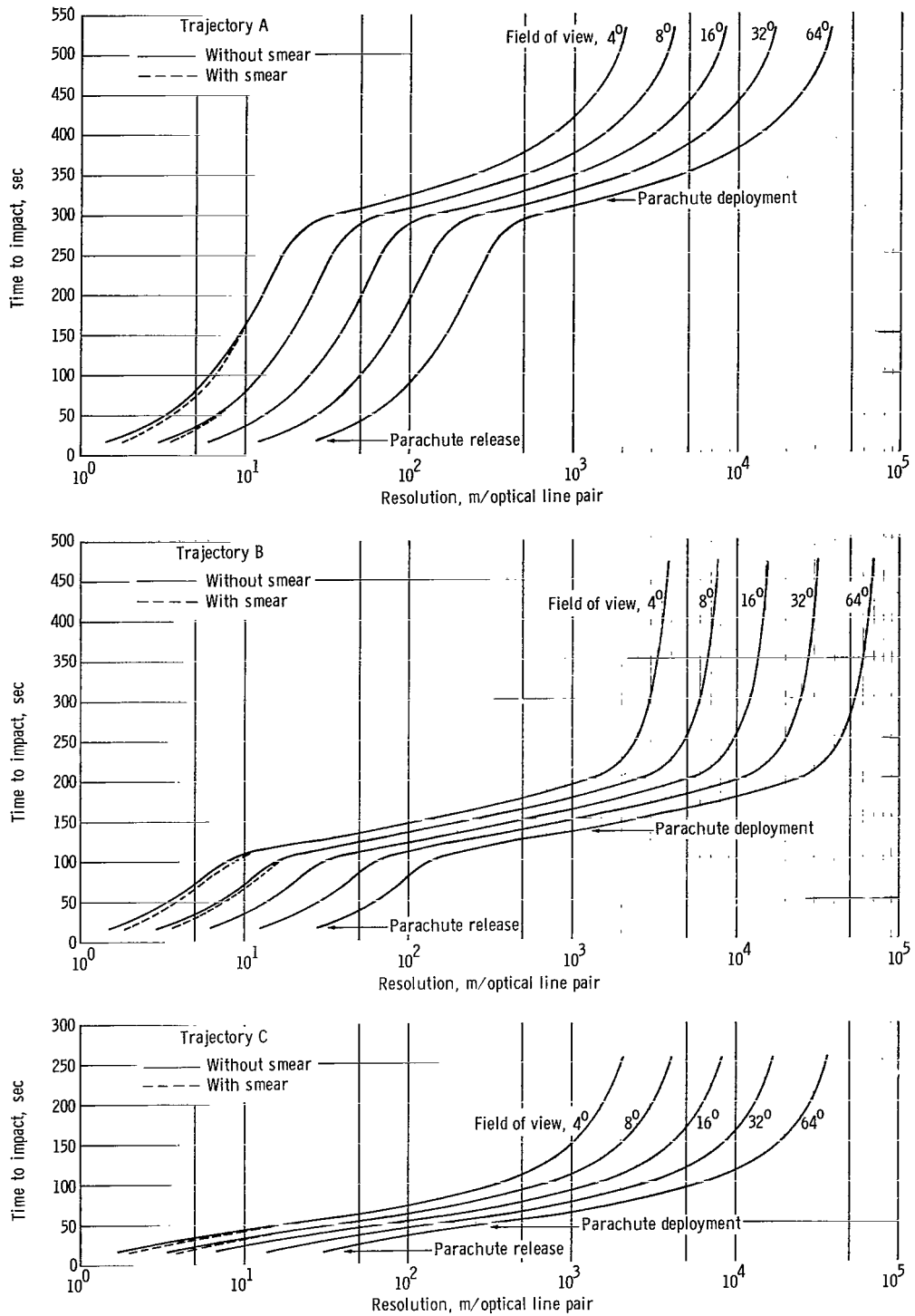


Figure 11.- Variation of surface resolution with time to impact for three descent trajectories. A 200-line television system and several lens field-of-view values are assumed. The television optical axis is aligned with the spacecraft center line. Smear is given for an exposure time of 5 msec and includes the effect of a 60-m/sec surface wind blowing in the direction of the flight path.

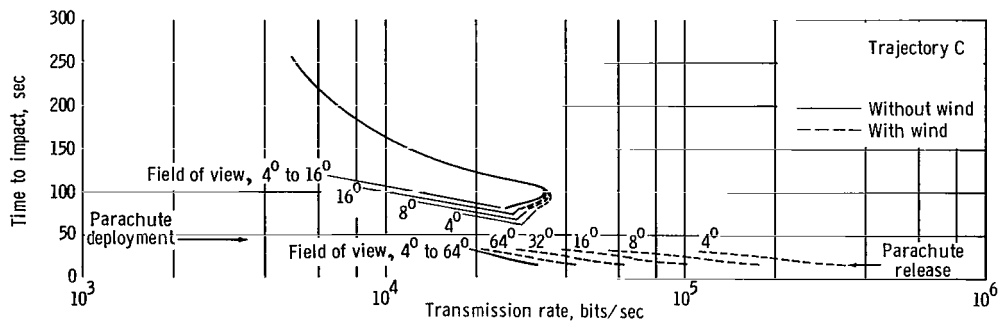
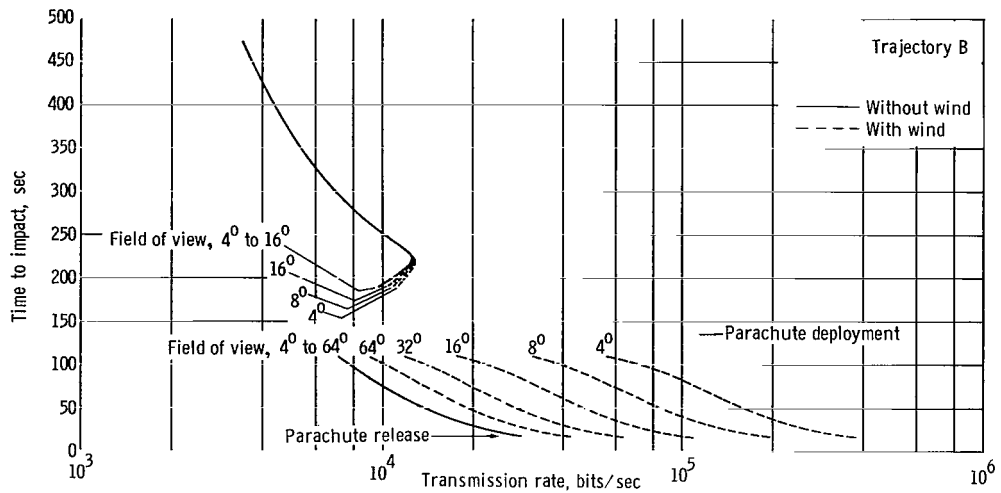
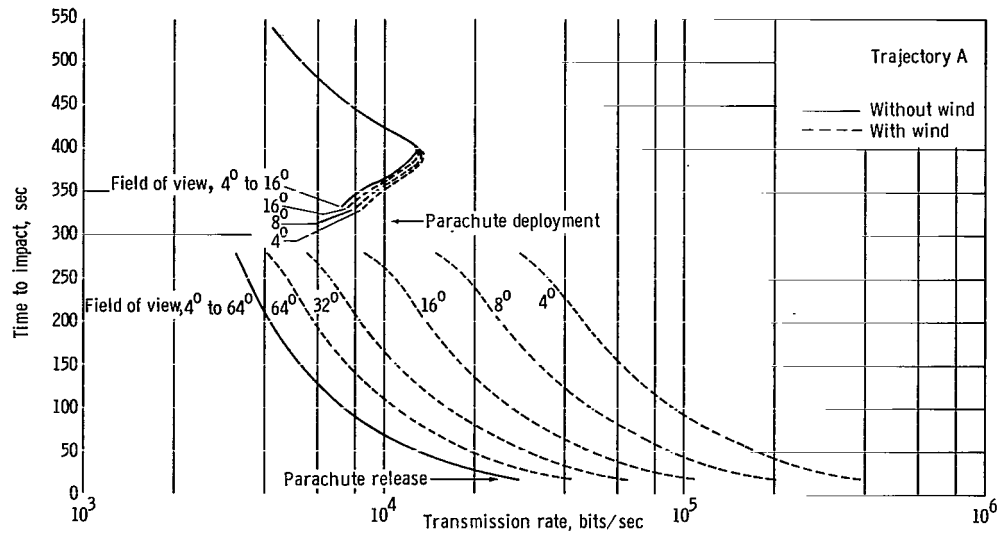
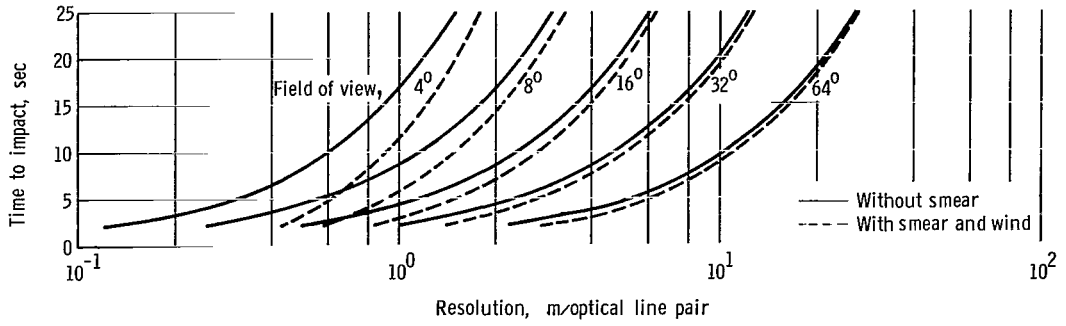
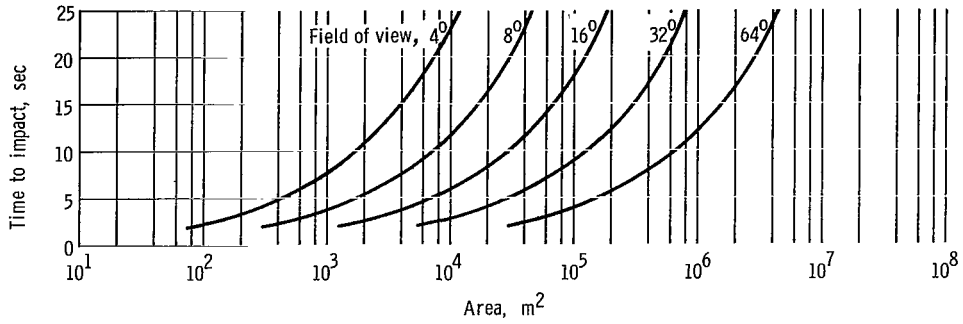


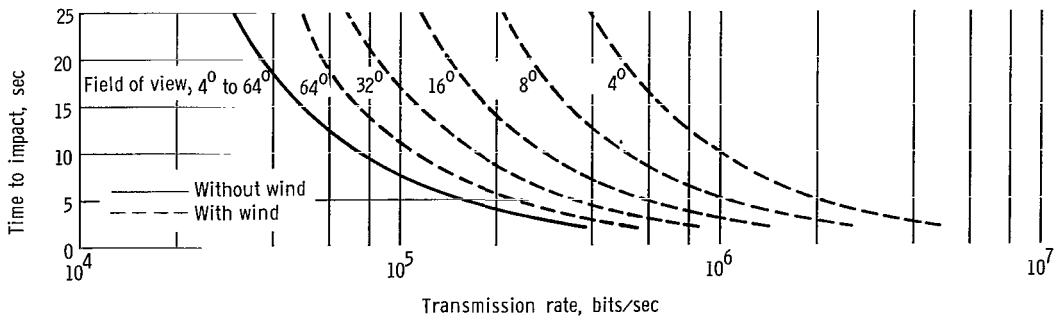
Figure 12.- Variation of transmission rate to achieve overlap of successive pictures with time to impact for three descent trajectories. A 200-line television system and several lens field-of-view values are assumed. The optical axis is aligned with the spacecraft center line. Transmission rate is given for the absence and presence of a 60-m/sec surface wind blowing in the direction of the flight path.



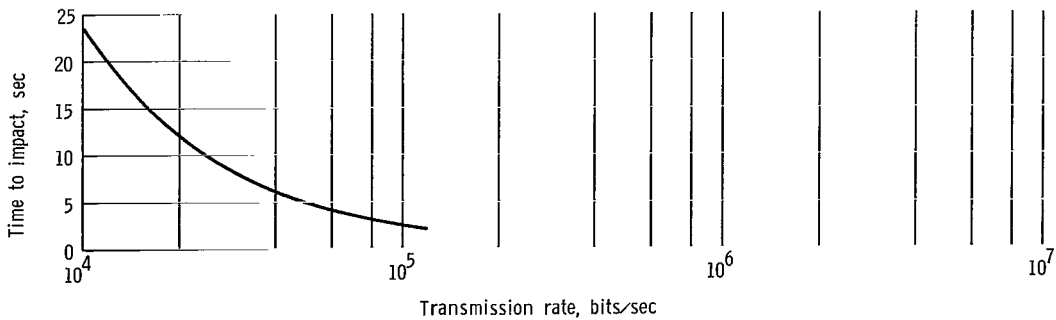
(a) Surface resolution.



(b) Area coverage.



(c) Transmission rate required to overlap successive pictures.



(d) Transmission rate required to transmit before impact.

Figure 13.- Variation of surface resolution, area coverage, and transmission rate with time to impact during the terminal descent phase. A 200-line television system and several lens field-of-view values are considered. A constant vertical spacecraft velocity of 60-m/sec is assumed. Absence and presence of a 60-m/sec surface wind are considered.

Transmission rate required to:

- Transmit a picture with a resolution of 1 meter before touchdown.
- Overlap successive pictures during terminal descent phase; effect due to surface wind excluded.
- ◇ Overlap successive pictures during aerodynamic decelerator phase; effect due to 60-m/sec surface wind included.
- △ Overlap successive pictures during ballistic entry phase; near vertical viewing geometry is assumed.

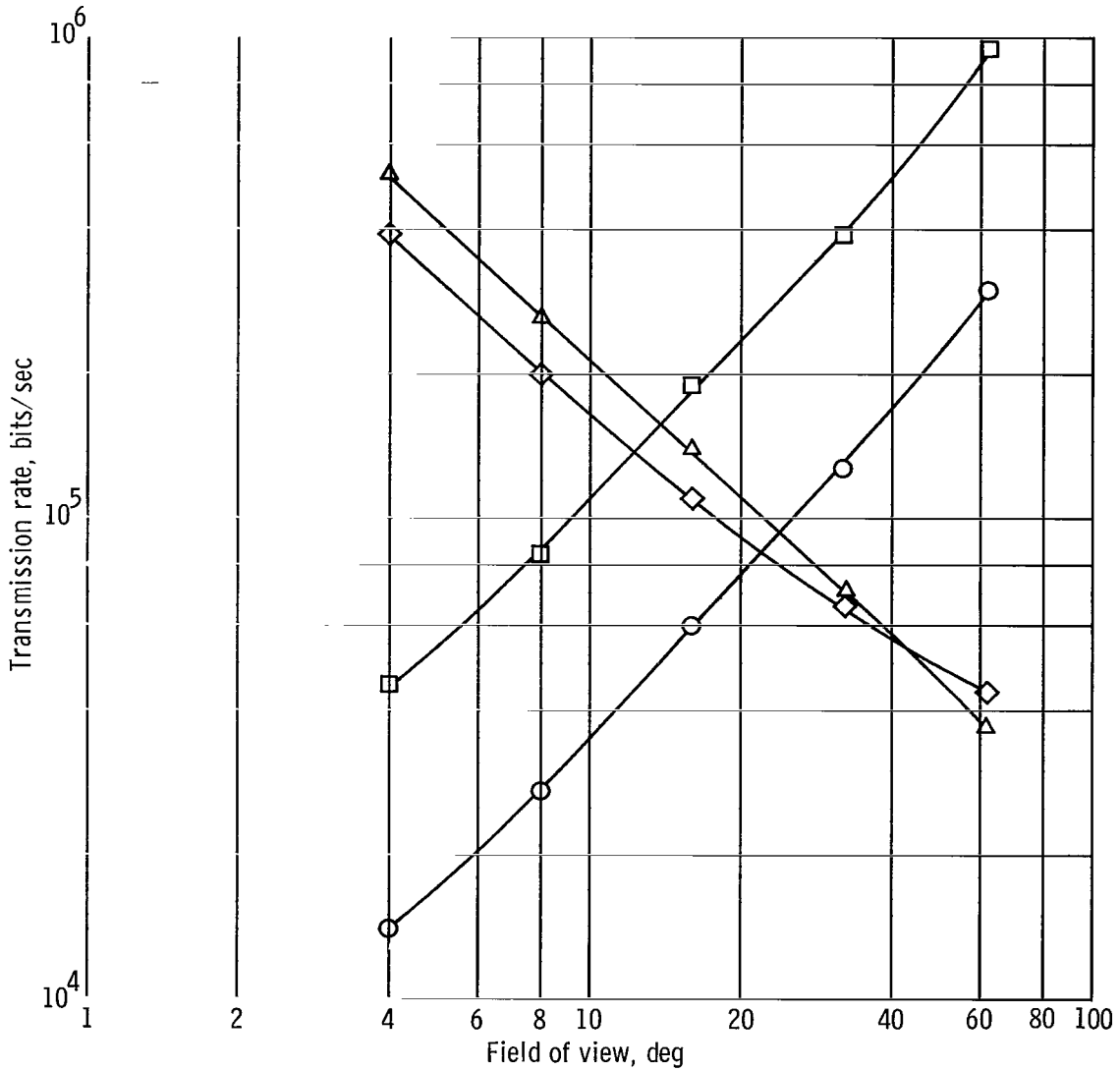


Figure 14.- Graphical solution for finding the field of view which minimizes the transmission rate required for a 200-line television system to accomplish the mission objectives. Trajectory A is considered.

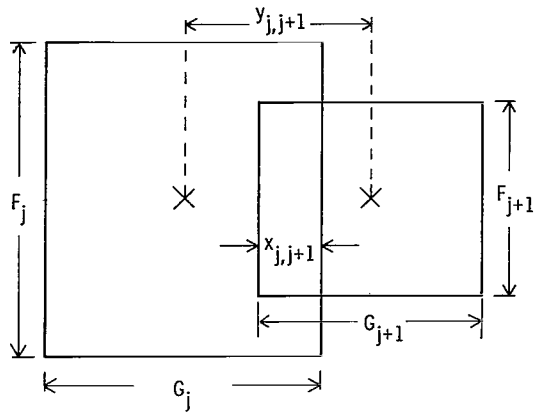


Figure 15.- Illustration of overlap requirement.

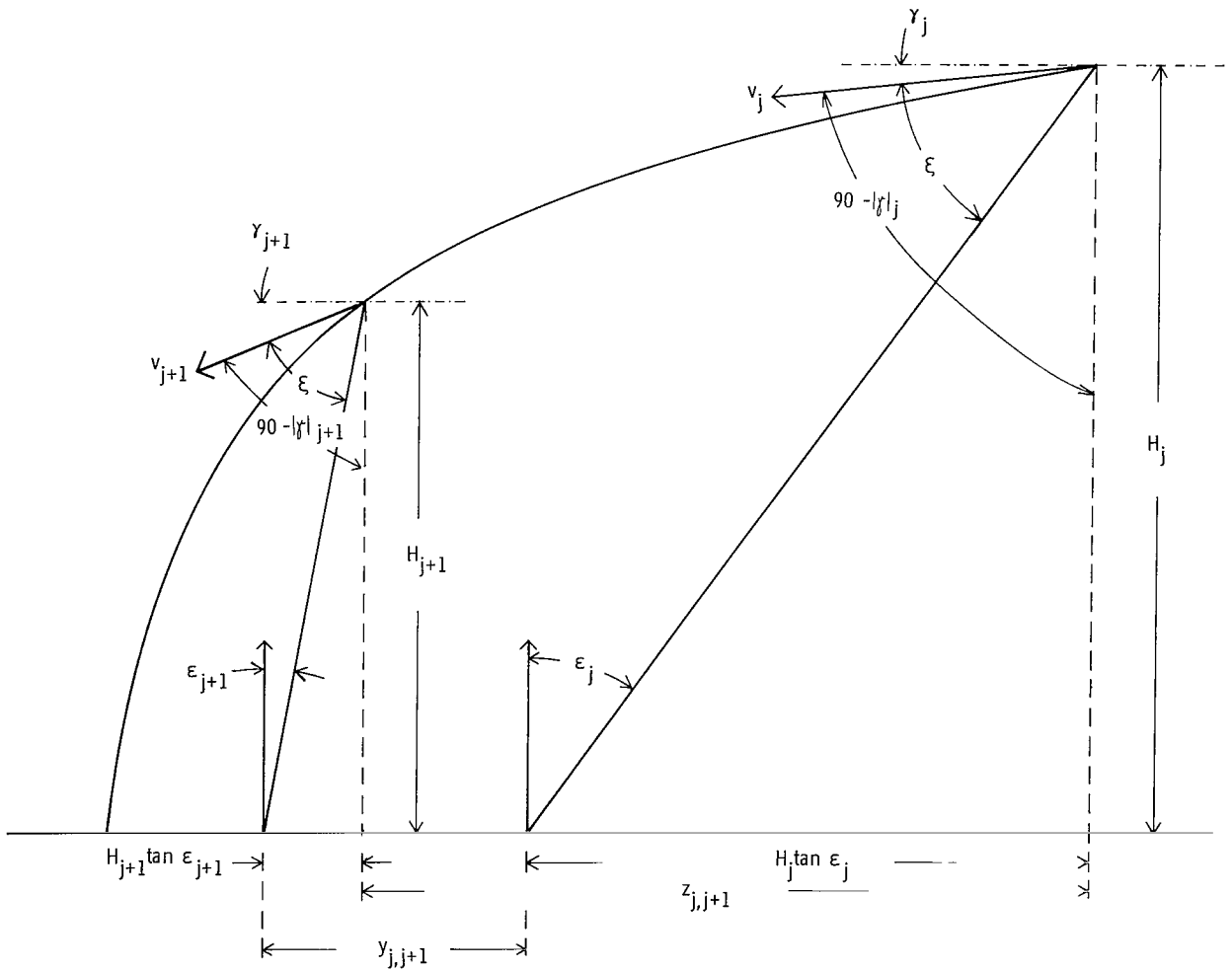


Figure 16.- Camera viewing geometry for two successive pictures.

FIRST CLASS MAIL

POSTMASTER: If Undeliverable (Section 158  
Postal Manual) Do Not Return

*"The aeronautical and space activities of the United States shall be conducted so as to contribute . . . to the expansion of human knowledge of phenomena in the atmosphere and space. The Administration shall provide for the widest practicable and appropriate dissemination of information concerning its activities and the results thereof."*

— NATIONAL AERONAUTICS AND SPACE ACT OF 1958

## NASA SCIENTIFIC AND TECHNICAL PUBLICATIONS

**TECHNICAL REPORTS:** Scientific and technical information considered important, complete, and a lasting contribution to existing knowledge.

**TECHNICAL NOTES:** Information less broad in scope but nevertheless of importance as a contribution to existing knowledge.

**TECHNICAL MEMORANDUMS:** Information receiving limited distribution because of preliminary data, security classification, or other reasons.

**CONTRACTOR REPORTS:** Scientific and technical information generated under a NASA contract or grant and considered an important contribution to existing knowledge.

**TECHNICAL TRANSLATIONS:** Information published in a foreign language considered to merit NASA distribution in English.

**SPECIAL PUBLICATIONS:** Information derived from or of value to NASA activities. Publications include conference proceedings, monographs, data compilations, handbooks, sourcebooks, and special bibliographies.

**TECHNOLOGY UTILIZATION PUBLICATIONS:** Information on technology used by NASA that may be of particular interest in commercial and other non-aerospace applications. Publications include Tech Briefs, Technology Utilization Reports and Notes, and Technology Surveys.

*Details on the availability of these publications may be obtained from:*

**SCIENTIFIC AND TECHNICAL INFORMATION DIVISION  
NATIONAL AERONAUTICS AND SPACE ADMINISTRATION  
Washington, D.C. 20546**